Control Engineering Practice 18 (2010) 944–953

Contents lists available at ScienceDirect

Control Engineering Practice

journal homepage: www.elsevier.com/locate/conengprac

Real-time seam tracking for robotic laser welding using trajectory-based control

Menno de Graaf *, Ronald Aarts, Ben Jonker, Johan Meijer

University of Twente, Laboratory of Mechanical Automation, P.O. Box 217, 7500 AE Enschede, The Netherlands

ARTICLE INFO

Article history:
Received 23 November 2007
Accepted 1 April 2010

Keywords:
Robotics
Seam tracking
Laser welding
Trajectory-based control
Trajectory generation
Synchronisation

ABSTRACT

In this paper a real-time seam tracking algorithm is proposed that can cope with the accuracy demands of robotic laser welding. A trajectory-based control architecture is presented, which had to be developed for this seam tracking algorithm. Cartesian locations (position and orientation) are added to the robot trajectory during the robot motion. In this way, sensor information obtained during the robot motion is used to generate the robot trajectory while moving. Experiments have been performed to prove the tracking capabilities of the seam tracking algorithm.

1. Introduction

Accurate path tracking of 3D trajectories using image-based sensors has received considerable attention in recent years. It is a task that is difficult to achieve for industrial robots. An application where this plays an important role is robotic laser welding. Laser welding requires high accuracies of the position of the laser focal point with respect to the seam trajectory. Accuracies down to 0.2 mm have to be achieved at welding speeds up to 250 mm/s. Therefore seam-tracking sensors, that measure the seam trajectory close to the laser focal spot, are required (Huissoon, 2002). The integration, however, of such sensors in a robotic system is not straightforward.

This paper considers real-time seam tracking for 3D seams. When the sensor is mounted some distance in front of the laser focal point it can measure the seam trajectory and let the laser focal point track the measured trajectory in the same movement. In the literature, many publications can be found that apply seam tracking to robotic arc welding, where the accuracy requirements (± 2 mm) are less stringent than for laser welding (Bae, Lee, & Ahn, 2002; Kim, Son, Cho, & Koh, 1996; Kim, Rhee, & Lee, 1999; Nayak & Ray, 1993; Yu & Na, 1997, 1998). Andersen (2001) and Fridenfalk and Bolmsjö (2003) show the application of seam tracking for robotic laser welding. Unfortunately, Andersen (2001) gives no technical details of his algorithms. Fridenfalk and Bolmsjö (2003) describe their algorithm but do not pay attention to robot integration aspects (e.g. robot-sensor synchronisation). Their system is an order of magnitude less accurate (± 2 mm) than what is aimed at in this work.

Seam tracking can be regarded as a form of visual servoing, which is the research area that considers the use of cameras and image-based sensors inside the control-loop of robots and manipulators. Two control architectures (Sanderson & Weiss, 1980) are distinguished in the visual servoing literature: position-based control and image-based control. In position-based control, features are extracted from the camera and used in conjunction with a geometric model of the target to determine the pose of the target with respect to the camera. In image-based control, the last step is omitted and servoing is done on the basis of image features directly.

The image-based approach may reduce computational delay, eliminate the necessity for image interpretation and eliminate errors in sensor modelling and camera calibration. However, it does present a significant challenge to controller design since the plant is non-linear and highly coupled. An advantage of image-based control is the relative robustness in the presence of image distortions and kinematic parameter variations in the manipulator Jacobian (Corke, 1994). For seam tracking, the position-based approach appears to be more straightforward as both feature detection and pose determination are already performed by the sensor. However, this approach does not take into account that typical process applications like welding and painting are normally done at a prescribed velocity, so an additional trajectory generator is needed to smoothly compute the desired pose at fixed time intervals in such a way that the velocity remains constant.

* Corresponding author. Tel.: +31 33 4950225.
E-mail address: menno@degraaf-slot.nl (M. de Graaf).

0967-0661/$ - see front matter © 2010 Elsevier Ltd. All rights reserved.
doi:10.1016/j.conengprac.2010.04.001

To apply either position-based or image-based control for seam tracking of 3D seam trajectories for laser welding at high velocities is difficult to achieve. Both control strategies use the sensor measurements from a camera directly within the time-based control-loop of the robot controller. To guarantee stability, the time delays that occur in the system (communication time, image acquisition time and image processing time) are part of the feedback loop and need to be accurately known (Liu, Hoover, & Walker, 2004). The sensor and robot usually have different cycle times, so synchronisation and interpolation need proper attention (De Graaf, 2007; De Graaf, Aarts, Meijer, & Jonker, 2005; Liu et al., 2004). To summarise, standard visual servoing techniques have a number of shortcomings if they are applied to seam tracking for robotic laser welding. In this paper, a trajectory-based solution will be presented. In the trajectory-based control strategy, new sensor measurements are obtained during the robot motion. These measurements are related to the robot position and added to a buffer to build a geometric seam trajectory. Simultaneously, a real-time trajectory generator is used to move the laser focal point with a prescribed velocity along the seam locations in the buffer. A real-time seam tracking algorithm filters and corrects the orientation of the seam locations to keep the sensor on a pre-defined trajectory, to decrease the effect of measurement noise and to smoothen the robot motion.

The paper starts with an overview of the coordinate frames and transformations that are used in a sensor-guided robotic laser welding unit. Section 3 presents the trajectory-based control structure. In Section 4 the real-time seam tracking algorithm is described. Experiments have been performed to show the ability of the algorithm for tracking and welding (Section 5). Finally, the results are discussed.

2. Coordinate frames and transformations

An overview of the coordinate frames and transformations that can be distinguished in a sensor-guided robotic welding system can be found in Nayak and Ray (1993). Their overview is generalised, by adding a station frame **M** and a product frame **H** (Fig. 1).

A transformation describes the location (position and orientation) of a frame with respect to a reference frame. Transformations are indicated by the symbol **T** with a leading superscript that defines the reference frame they refer to. The leading subscript defines the frame they describe, e.g. transformation ${}^{A}_{B}\mathbf{T}$ describes frame **B** with respect to frame **A**. A homogenous transformation matrix is used to describe a transformation. It consists of a 3×3 rotation matrix and 3D position vector and can be written as

$$ {}^{A}_{B}\mathbf{T} = \begin{bmatrix} {}^{A}_{B}\mathbf{R} & {}^{A}_{B}\mathbf{P} \\ \mathbf{0} & 1 \end{bmatrix}, \tag{1} $$

where ${}^{A}_{B}\mathbf{R}$ is the rotation matrix and ${}^{A}_{B}\mathbf{P}$ the position vector that describe the orientation and position of frame **B** relative to frame **A**.

In Fig. 1 the following frames are defined:

- **B:** Base or world frame. This frame is attached to the robot base and does not move with respect to the environment.
- **N:** Null frame. The null frame is located at the robot end-effector or the end of the robot flange. The null frame is described with respect to the base frame by coordinate transformation ${}^{B}_{N}\mathbf{T}$, which is a function of the joint positions of the robot arm.
- **L:** Laser tool frame. The laser tool frame is located at the focal point of the laser beam. The *z*-axis of this frame coincides with the laser beam axis. Because the laser beam is axi-symmetric, the direction of the *x*-axis is arbitrary, unless the symmetry is broken due to e.g. the presence of peripheral equipment. Without of loss of generality it will be chosen in the direction of the sensor tool frame in this work. The transformation ${}^{N}_{L}\mathbf{T}$ describes the laser tool frame with respect to the null frame. This is a fixed transformation determined by the geometry of the welding head.
- **S:** Sensor tool frame. The seam tracking sensor is fixed to the welding head and therefore indirectly to the robot flange. The transformation ${}^{N}_{S}\mathbf{T}$ describes the sensor tool frame with respect to the null frame. Note that, because both transformations are fixed, this transformation can also be described with respect to the laser tool frame instead of the null frame by transformation ${}^{L}_{S}\mathbf{T}$.
- **M:** Station frame. The station frame is the base of the station or work table a product is attached to. It is possible that the product is clamped on a manipulator which moves the product with respect to the base frame. In that case the transformation ${}^{B}_{M}\mathbf{T}$ describes the station frame with respect to the base frame and depends on the joint values of the manipulator.
- **H:** Product frame. The product frame is located on a product. The transformation ${}^{M}_{H}\mathbf{T}$ describes the product frame with respect to the station frame. This frame is useful if a series of similar products are welded on different locations of a station.
- **G:** Seam frame. Every discrete point on a seam can be described with a different coordinate frame. The transformation ${}^{H}_{G}\mathbf{T}$ describes a seam frame with respect to the product frame. The mathematical description of the seam will be discussed in more detail in Section 4.2.
- **T:** Robotic tool frame. A general robot movement is specified by the movement of a robotic tool frame **T**, which can be either the sensor tool frame **S** or laser tool frame **L**. Some equations that are derived in this work account for either **S** or **L**. In that case the symbol **T** will be used.
- **F:** Robotic frame. A general robot movement is specified with respect to a frame **F**, which can be the base frame **B**, station frame **M**, product frame **H** or seam frame **G**. The symbol **F** will be used in general equations that account for all of these frames.

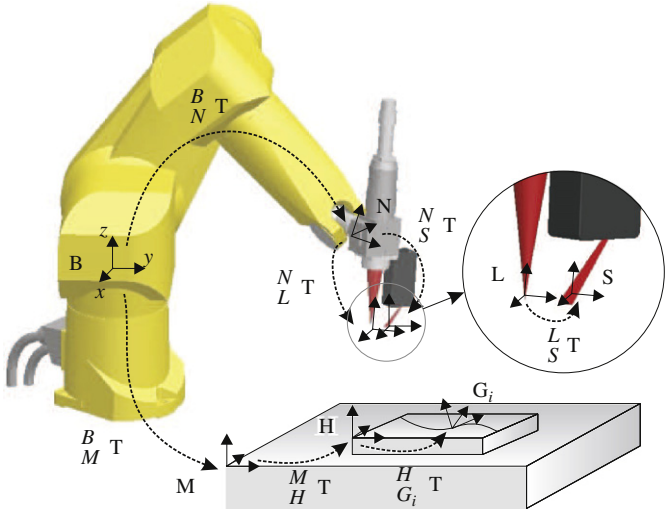

Fig. 1. Frames and transformations for sensor-guided robotic laser welding.

If the seam trajectory is within the field-of-view of the seam-tracking sensor, it can measure a location ${}^{S}_{G}\mathbf{T}$ on the seam trajectory with respect to its coordinate frame **S**. In general, a seam-tracking sensor does not measure the complete position and

orientation coordinates of each location and multiple measurements are combined as will be outlined in Section 4.2. Next this seam location can be computed with respect to generic frame **F** as

$$ {}^{F}_{G}\mathbf{T} = {}^{B}_{F}\mathbf{T}^{-1}\,{}^{B}_{N}\mathbf{T}\cdot{}^{N}_{S}\mathbf{T}\cdot{}^{S}_{G}\mathbf{T}, \tag{2} $$

where ${}^{B}_{F}\mathbf{T}$ is a known transformation from the robot base frame **B** to the generic frame **F** and ${}^{N}_{S}\mathbf{T}$ is a known fixed transformation from robot flange frame **N** to the sensor frame **S**. Transformation ${}^{B}_{N}\mathbf{T}$ is calculated from the measured robot joint angles $\mathbf{q}_m$ as

$$ {}^{B}_{N}\mathbf{T} = DGM(\mathbf{q}_m), \tag{3} $$

where *DGM*( ) depends on the geometry of the robot arm (e.g. arm lengths, encoder offsets). In the literature *DGM*( ) is often called the forward kinematics function (Craig, 1986) or Direct Geometric Model (Khalil & Dombre, 2002). Khalil and Dombre have derived symbolic expressions for computing Eq. (3) in the specific case of the 6-axes Stäubli robot used in this work.

Transformation ${}^{S}_{G}\mathbf{T}$ is computed from a sensor image using image processing (De Graaf, 2007). If the robot is moving, the transformations ${}^{B}_{N}\mathbf{T}$ and ${}^{S}_{G}\mathbf{T}$ change in time. To accurately compute a seam location ${}^{F}_{G}\mathbf{T}$, the robot joint measurements need to be synchronised with the sensor image acquisition.

3. Trajectory-based control

Fig. 2 shows a block diagram of the trajectory-based control strategy proposed in this paper. The top part of this figure contains the robot trajectory generation, the bottom part contains the sensor integration part. Fig. 2 will be explained, starting from the top left part.

The Tool Trajectory Buffer contains a list of locations (positions and orientations) that the robot tool frame **T** (which can be **S** or **L**) has to pass through during the robot motion. These locations do not need to be equidistant. During the robot motion new locations can be added to the Tool Trajectory Buffer, thus extending the robot trajectory.

A real-time Setpoint Generator interpolates the locations in the Tool Trajectory Buffer and computes location setpoints ${}^{F}_{T}\mathbf{T}_k$ for every k th fixed time interval (4 ms in our case). The movement should be smooth as defined by the maximum acceleration, velocity and deceleration specified in the Motion descriptor. Several publications on trajectory generation can be found in the literature. Ahmed Bazaz and Tondu (1999) have presented a real-time trajectory generator that interpolates the trajectory in the joint-space. Khalil and Dombre (2002) describe a theoretical framework for real-time trajectory generation in Cartesian space. Unfortunately, only the positional part of the trajectory generation is worked out in detail in their framework. Abo-Hammour, Mirza, Mirza, and Arif (2002) describe Cartesian path generation using continuous genetic algorithms, which does not necessarily pass exactly through the defined Tool Trajectory locations and lacks computational efficiency for real-time implementation. In this work, a real-time Setpoint Generator is used (De Graaf, 2007; De Graaf, Aarts, Jonker, & Meijer, 2006), which is based on the work of Sgarbi and Cammoun (1992). The trajectory is interpolated in Cartesian space and the velocity tracks a trapezoid profile.

From a location setpoint ${}^{F}_{T}\mathbf{T}_k$, the known tool frame transformation ${}^{N}_{T}\mathbf{T}$ and the known frame transformation ${}^{B}_{F}\mathbf{T}$, transformation ${}^{B}_{N}\mathbf{T}_k$ is computed as

$$ {}^{B}_{N}\mathbf{T}_k = {}^{B}_{F}\mathbf{T}\cdot{}^{F}_{T}\mathbf{T}_k\cdot{}^{N}_{T}\mathbf{T}^{-1}. \tag{4} $$

Next, a robot joint angle setpoint $\mathbf{q}^{d}_k$ is computed using the Inverse Geometric Model of the robot arm (Khalil & Dombre, 2002).

The robot joint angle setpoints $\mathbf{q}^{d}_k$ are the reference input for the Joint Motion Controller, which is proprietary to Stäubli. The motion controller must assure that the joint measurements $\mathbf{q}^{m}_k$ remain close to the specified reference, i.e. the tracking errors $|\mathbf{q}^{d}_k - \mathbf{q}^{m}_k|$ are small.

The seam tracking sensor determines the transformation ${}^{S}_{G}\mathbf{T}_i$ of a seam location somewhat ahead of the current laser tool frame location from a camera image using image-processing, where i is a measurement index. If properly synchronised (De Graaf, 2007; De Graaf et al., 2005), ${}^{S}_{G}\mathbf{T}_i$ can be related to the measured joint angles $\mathbf{q}^{m}_k$ to compute a seam location ${}^{F}_{G}\mathbf{T}_i$ using Eqs. (2) and (3). The result is stored in the Seam Trajectory Buffer. After the robot joints and sensor image are synchronised, the actual time upon which the seam locations were measured is not relevant anymore as the seam is defined by its geometric description only. Of course, the order in which the seam locations are obtained is of importance and it has to be assured that the number of points measured on the seam trajectory is sufficient in relation to the complexity of the seam. By moving the sensor tool frame along the seam trajectory and storing the obtained seam locations into the Seam Trajectory Buffer, the complete geometry of the seam trajectory is stored.

The loop can be closed by feeding data from the Seam Trajectory Buffer to the Tool Trajectory Buffer in which case 'smoothing and orientation correction' is necessary as will be detailed in Section 4.1. Information from a nominal trajectory may be used to provide smoothed data to the Tool Trajectory

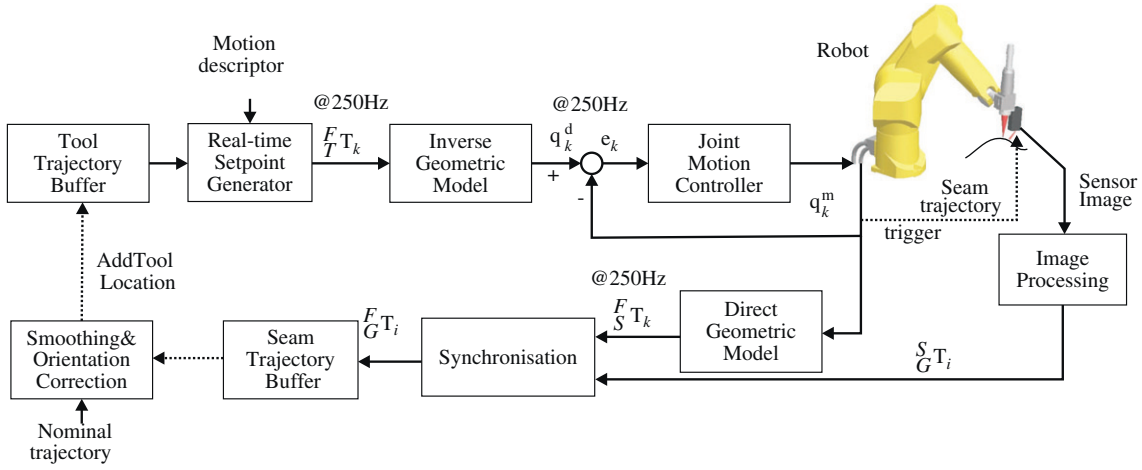

Fig. 2. Block diagram of trajectory-based control.

Buffer. The dashed lines in Fig. 2 indicate that it is not necessary that the data are exchanged at the rate of the real-time loop.

The trajectory-based control approach yields some major advantages, compared to common time-based control approaches:

- The measured locations in the Seam Trajectory Buffer can be filtered in the position-domain instead of in the time-domain. This is more logical as seam trajectories are characterised by their radius of curvature. Curvature is meaningful in the position-domain, not in the time or frequency domain.
- Both historic and future information is available for filtering as the sensor measures ahead of the laser focal point. Phase-coherent or central filtering can thus be applied easily.
- The sensor image processing is not part of the robot motion control loop. The control structure is therefore independent of a variable delay after processing of the sensor image which may be caused by the image processing algorithm. Furthermore, stability issues are properly decoupled this way.
- It is easy to remove outliers. The sensor measurements may be incorrect (due to dust, spatter from the process, etc.) or completely missing (due to sensor-robot communication errors). As long as the robot tool frame has not reached the end of the Tool Trajectory Buffer, the movement will continue.

The application of trajectory-based control for seam tracking is described in the next section.

4. Real-time seam tracking

4.1. Seam teaching and tracking

The trajectory-based control approach can be used for a number of different operations:

- teaching a seam trajectory, with prior knowledge of its geometry, e.g. from CAD-data;
- teaching an unknown seam trajectory;
- real-time tracking a seam trajectory, with prior knowledge of its geometry;
- real-time tracking an unknown seam trajectory.

The prior knowledge of the seam trajectory is included in the nominal seam trajectory, which is an approximation of the actual seam trajectory that the laser focal point has to track during laser welding. The nominal seam trajectory can be obtained in several ways:

- by manual programming;
- from a previous seam-teaching procedure;
- from a CAD file or Off-line programming software.

The seam locations of the nominal and actual seam trajectories are both stored in buffers that contain a number of seam locations. In practice, the nominal seam locations are expected to be within a few millimetres from the actual seam trajectory, which implies that if the sensor is positioned on the nominal seam trajectory, the actual seam trajectory is in the sensor's field-of-view.

The trajectory-based control structure only differs slightly for the above-mentioned seam teaching and seam tracking operations. In the case of teaching of a seam trajectory, with prior knowledge of its geometry, the smoothing and orientation correction block in Fig. 2 is not used, because the Tool Trajectory locations are known beforehand and the Seam Trajectory only needs to be recorded. For the other three procedures, the control loop has to be closed by on-line calculation and addition of locations to the Tool Trajectory Buffer. A proper smoothing must be taken care of to prevent oscillatory motion behaviour, because the trajectory-based control strategy contains no other bandwidth limitations. In the case of teaching an unknown seam trajectory, the Tool Trajectory Buffer needs to be filled with estimated seam locations, somewhere ahead of the current sensor location, which are extrapolated from the measured seam locations.

For real-time tracking of a seam trajectory, the sensor is used to obtain the location of the actual seam trajectory. The laser spot needs to be kept on this seam trajectory. Obviously, the seam trajectory has to remain in the sensors field-of-view, e.g. by rotating slightly around the laser tool frame origin. Real-time seam tracking without any prior knowledge of the geometry of the seam trajectory is considered to be impractical for safety reasons. In this work, real-time seam tracking is only performed when a nominal seam trajectory is already present to prevent the welding head hitting obstacles in the work cell due to erroneous sensor measurements, e.g. scratches. Only small deviations from a nominal trajectory are allowed. The nominal seam trajectory will be kept in the sensors field-of-view to make sure its measurements can be used.

4.2. Seam model

A seam trajectory can be considered as a continuous curve in 3D space (Fig. 3). From a mathematical point of view, the position of a discrete point n on the seam trajectory can be described by a 3D vector $\mathbf{P}_n$. The modelled seam trajectory should also include a description of the orientation. The orientation of a discrete point on the seam trajectory is described by the surface normal $\mathbf{n}_n$ of the workpiece. Note that the surface normal in a single point on a seam trajectory does not provide information about the direction along the seam trajectory. This direction can only be determined if at least 2 points (and their order) are known.

The seam model shown in Fig. 3 is defined by choosing a number of discrete points on the seam trajectory that each consist of a position vector and a surface normal. In a product, the seam trajectory is continuous. Therefore the seam trajectory will be interpolated between the discrete base points. A segment-wise cubic parametric spline of the form

$$^{F}\mathbf{K}_n(\lambda)=\begin{bmatrix}^{F}\mathbf{P}_n(\lambda)\\ ^{F}\mathbf{n}_n(\lambda)\end{bmatrix}=\mathbf{a}_n\lambda^3+\mathbf{b}_n\lambda^2+\mathbf{c}_n\lambda+\mathbf{d}_n \tag{5}$$

is chosen as the interpolation function, where $^{F}\mathbf{P}_n(\lambda)$ represents the position vector and $^{F}\mathbf{n}_n(\lambda)$ the surface normal with respect to frame **F**. The coefficients on the segment are calculated with the

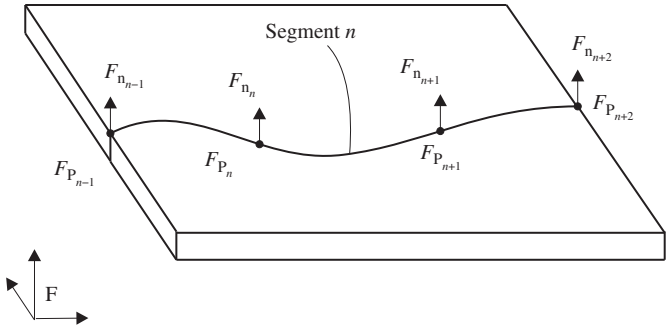

Fig. 3. Seam trajectory model.

Catmull–Rom expression (Barnhill & Riesenfeld, 1974) as

$$\begin{bmatrix} \mathbf{a}_n^T \\ \mathbf{b}_n^T \\ \mathbf{c}_n^T \\ \mathbf{d}_n^T \end{bmatrix} = \frac{1}{2} \begin{bmatrix} -1 & 3 & -3 & 1 \\ 2 & -5 & 4 & -1 \\ -1 & 0 & 1 & 0 \\ 0 & 2 & 0 & 0 \end{bmatrix} \begin{bmatrix} {}^F\mathbf{K}_{n-1}^T \\ {}^F\mathbf{K}_n^T \\ {}^F\mathbf{K}_{n+1}^T \\ {}^F\mathbf{K}_{n+2}^T \end{bmatrix}. \quad (6)$$

Given a spline segment n between ${}^F\mathbf{K}_n$ and ${}^F\mathbf{K}_{n+1}$ as shown in Fig. 3, four base points are needed to calculate the spline coefficients $\mathbf{a}_n$, $\mathbf{b}_n$, $\mathbf{c}_n$ and $\mathbf{d}_n$. The spline-functions of Eq. (5) exist between the start of segment n at $\lambda=0$ (where ${}^F\mathbf{P}_n(0)={}^F\mathbf{P}_n$ and ${}^F\mathbf{n}_n(0)={}^F\mathbf{n}_n$) and the end of the segment at $\lambda=1$ (where ${}^F\mathbf{P}_n(1)={}^F\mathbf{P}_{n+1}$ and ${}^F\mathbf{n}_n(1)={}^F\mathbf{n}_{n+1}$). An advantage of the cubic spline is that it can be used to interpolate complex trajectories with a small number of base points. Another useful property of the spline is its smoothness, because the first derivative of the interpolation function is continuous at the boundaries of the interval.

At the first and last segments of the seam trajectory, ${}^F\mathbf{K}_{n-1}$ and ${}^F\mathbf{K}_{n+2}$, respectively, are not available. In order to calculate the spline coefficients in these cases, virtual points ${}^F\mathbf{K}_{n-1}$ and ${}^F\mathbf{K}_{n+2}$ are used, which are computed by linearly extrapolating as

$${}^F\mathbf{K}_{n-1} = 2{}^F\mathbf{K}_n - {}^F\mathbf{K}_{n+1} \quad (7)$$

for the first segment and

$${}^F\mathbf{K}_{n+2} = 2{}^F\mathbf{K}_{n+1} - {}^F\mathbf{K}_n \quad (8)$$

for the last segment. If the seam trajectory consists only of two base points, Eq. (5) reduces from cubic interpolation to linear interpolation ($\mathbf{a}_n=\mathbf{b}_n=0$) this way.

4.3. Real-time seam tracking algorithm

The real-time seam tracking procedure can be divided into two subsequent steps (Fig. 4). First, the sensor is positioned at the starting point of the nominal seam trajectory. The sensor is moved along the nominal seam trajectory for a certain distance (the look-ahead distance), while the actual seam trajectory is measured. During this step, only the positioning of the sensor tool frame is of importance as laser processing does not take place yet. Once the first part of the actual seam trajectory is known, the laser focal point will be positioned at the starting point of the actual seam trajectory. During the second step, the measured actual seam trajectory is welded, while the sensor simultaneously tracks the nominal seam trajectory and measures the remaining part of the actual seam trajectory. Once the sensor has passed the end point of the nominal seam trajectory, no additional locations will be added to the actual seam trajectory anymore. The remaining part of the actual seam trajectory will be welded using the last known orientation.

(1) To perform the first step, the look-ahead distance l has to be known, which is computed from the positional parts of the known sensor tool frame transformation ${}^N_S\mathbf{T}$ and laser tool frame transformation ${}^N_L\mathbf{T}$ as

$$l = |{}^L_S\mathbf{P}| = |{}^N_S\mathbf{P} - {}^N_L\mathbf{P}|. \quad (9)$$

The locations of the nominal seam trajectory that are within a distance l from the start of the nominal seam trajectory are added to the Tool Trajectory Buffer using the sensor tool frame transformation ${}^N_S\mathbf{T}$. The sensor is moved along this trajectory, while measuring the actual seam locations. These locations are stored in the Seam Trajectory Buffer to be welded in the second part of the procedure.
During the second part, the laser focal point has to be focussed on any of these locations, while keeping the sensor on the nominal seam trajectory. Therefore the orientation of these locations has to be corrected (Section 4.4). Furthermore, the corrected seam locations will be filtered (Section 4.5), to smoothen the robot motion, to decrease the influence of sensor noise and to prevent unstable motion behaviour.
At the end of the first step, the corrected and filtered actual seam locations are added to the Tool Trajectory Buffer using the laser tool frame transformation ${}^N_L\mathbf{T}$. The laser focal point is moved to the first location in the Tool Trajectory Buffer, which corresponds to the start point of the actual seam trajectory.

(2) In the second step, laser welding is performed and the laser focal point will move along the actual seam trajectory. During this movement, new seam locations are measured. The orientations of these seam locations are adjusted and filtered and the result is added to the Tool Trajectory Buffer. When the sensor moves past the end point of the nominal seam trajectory, no more locations will be added to the Tool Trajectory Buffer and the process continues until the laser focal point reaches the end of the Tool Trajectory Buffer.

To maintain a safe operation, the following safety conditions are applied:

- Synchronised seam locations are only added to the Seam Trajectory Buffer if they are at a minimal distance (typically 0.2 mm) from the previous seam location to make sure the seam locations are not too close at low robot speeds, so filtering is always performed with locations that are at a minimal distance.
- Invalid sensor measurements are automatically ignored, because they are not added to the Seam Trajectory Buffer. If a series of invalid sensor measurements occurs, the robot motion will eventually automatically stop when the laser focal point reaches the end of the Tool Trajectory Buffer.
- Filtered seam locations are only added to the Tool Trajectory Buffer, if they are within 3 mm of the nominal seam trajectory.

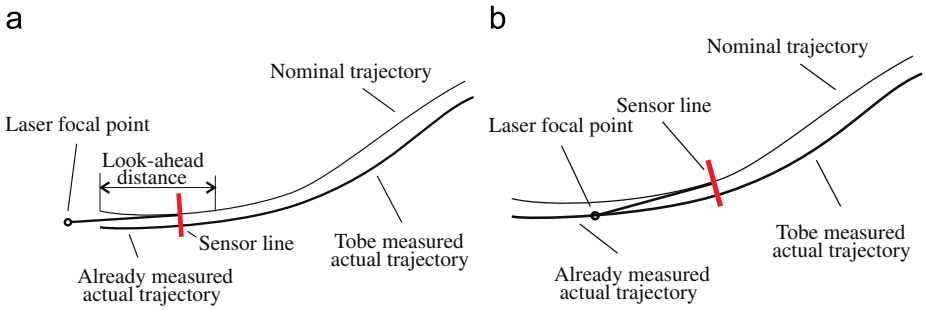

Fig. 4. Schematic overview of the real-time seamtracking algorithm. (a) Step 1: measuring the first part of the actual trajectory, (b) Step 2: tracking and welding.

4.4. Orientation correction

The orientation of the locations in the Seam Trajectory Buffer will be corrected in such a way that if the laser focal point is positioned at a seam location, the sensor tool frame intersects the nominal seam trajectory. This is illustrated in Fig. 5, where the sensor measures a seam location ${}^F_G\mathbf{T}_i$ on the actual seam trajectory.

When the laser focal point reaches location ${}^F_G\mathbf{T}_i$, its rotational part ${}^F_G\mathbf{R}_i$ should be such that the sensor intersects the nominal trajectory at position ${}^F\mathbf{P}_n(\lambda^{\text{int}})$, which is at a distance l from the origin of ${}^F_G\mathbf{T}_i$, so

$$|{}^F\mathbf{P}_n(\lambda^{\text{int}}) - {}^F_G\mathbf{P}_i| = l. \tag{10}$$

The intersection ${}^F\mathbf{P}_n(\lambda^{\text{int}})$ is computed numerically using the seam model of the nominal trajectory. For segment n on the nominal trajectory, which contains the intersection ${}^F\mathbf{P}_n(\lambda^{\text{int}})$, the following two conditions apply:

$$|{}^F\mathbf{P}_n - {}^F_G\mathbf{P}_i| \le l \tag{11}$$

and

$$|{}^F\mathbf{P}_{n+1} - {}^F_G\mathbf{P}_i| \ge l, \tag{12}$$

where ${}^F\mathbf{P}_n$ and ${}^F\mathbf{P}_{n+1}$ are the positions on the nominal trajectory at the start and end of segment n.

Using Eq. (5), the position ${}^F\mathbf{P}_n(\lambda)$ and its derivative $(\partial/\partial\lambda){}^F\mathbf{P}_n(\lambda)$ can be evaluated for any value of λ. An iterative Newton–Raphson root-finding method (Abramowitz & Stegun, 1972) is used to numerically compute the value of λ^{int} on the segment n that satisfies Eq. (10).

Once the intersection ${}^F\mathbf{P}_n(\lambda^{\text{int}})$ has been found, the remaining step is to compute the orientation such that the sensor tool frame origin indeed matches the intersection. Assume initially ${}^F_G\mathbf{R}_i^{\text{uncor}}$ uncorrected, then the corrected orientation ${}^F_G\mathbf{R}_i^{\text{cor}}$ can be computed as

$${}^F_G\mathbf{R}_i^{\text{cor}} = {}^F_G\mathbf{R}_i^{\text{uncor}}\,\mathbf{R}^{\text{rel}}, \tag{13}$$

where $\mathbf{R}^{\text{rel}}$ is the relative correction. If the laser tool frame origin is positioned at location ${}^F_G\mathbf{T}_i$, the intersection ${}^F\mathbf{P}_n(\lambda^{\text{int}})$ can be computed relative to the laser frame using

$$\begin{bmatrix} {}^L\mathbf{P}_n(\lambda^{\text{int}}) \\ 1 \end{bmatrix} = {}^F_G\mathbf{T}_i^{-1} \begin{bmatrix} {}^F\mathbf{P}_n(\lambda^{\text{int}}) \\ 1 \end{bmatrix}. \tag{14}$$

The position ${}^L_S\mathbf{P}$ of the sensor frame relative to the laser frame is computed from the known laser tool frame transformation ${}^N_L\mathbf{T}$ and sensor tool frame transformation ${}^N_S\mathbf{T}$ using Eq. (9). Obviously, the laser tool frame location has to be adjusted such that the local position of the sensor frame ${}^L_S\mathbf{P}$ coincides with the intersection ${}^L\mathbf{P}_n(\lambda^{\text{int}})$. Using the vectors ${}^L\mathbf{P}_n(\lambda^{\text{int}})$ and ${}^L_S\mathbf{P}$, the orientation can be expressed as a rotation with angle θ around a unit 3D vector $\mathbf{u}$, where the angle θ between the vectors is computed as

$$\theta = \arccos\left(\frac{{}^L\mathbf{P}_n(\lambda^{\text{int}})}{|{}^L\mathbf{P}_n(\lambda^{\text{int}})|} \cdot \frac{{}^L_S\mathbf{P}}{|{}^L_S\mathbf{P}|}\right), \tag{15}$$

and the unit vector $\mathbf{u}$, which is normal to both vectors, is computed as

$$\mathbf{u} = \frac{{}^L\mathbf{P}_n(\lambda^{\text{int}}) \times {}^L_S\mathbf{P}}{|{}^L\mathbf{P}_n(\lambda^{\text{int}}) \times {}^L_S\mathbf{P}|}. \tag{16}$$

Obviously no rotation correction is needed if $\theta \approx 0$, which means that the two vectors are already in line with each other. The relative rotation matrix $\mathbf{R}^{\text{rel}}$ can be computed from $\mathbf{u}$ and θ, e.g. using standard quaternion algebra.

In practice, there are two cases in which there is no intersection of the sensor with the nominal seam trajectory.

- If the length of the total nominal seam trajectory is smaller than the lookahead distance, the sensor has already passed the end of the nominal seam trajectory once the laser reaches the start of the actual trajectory. In this case no orientation correction is applied.
- If the distance between the current laser tool frame origin and the end of the nominal seam trajectory is smaller than the lookahead distance, the sensor has passed the end of the seam trajectory. In this case, the last applied orientation correction is maintained.

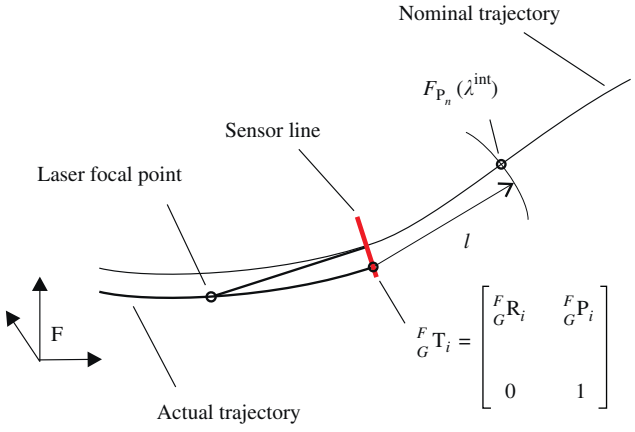

Fig. 5. Orientation correction during real-time seamtracking.

4.5. Filtering

The corrected seam locations contain noise and may be close to each other, especially if the robot moves at slow speeds. They cannot be directly added to the Tool Trajectory Buffer, because by design, the trajectory-based control strategy does not limit the bandwidth. Consequently noise would result in an irregular robot motion as the Setpoint Generator interpolates a tool trajectory that passes exactly through the specified Tool Trajectory locations.

Therefore, the corrected seam locations will be filtered and only added to the Tool Trajectory Buffer if they are at a minimal distance from each other. The positions and orientations in the Seam Trajectory Buffer are filtered separately. For the position, a polynomial of order n will be used, which has the form

$$\mathbf{P}(p) = \mathbf{a}_n p^n + \mathbf{a}_{n-1} p^{n-1} + \cdots + \mathbf{a}_1 p + \mathbf{a}_0. \tag{17}$$

In practice, a polynomial order $n=2$ is used. The filtered seam locations are not needed until the laser focal point reaches them. Therefore, both historic and future seam locations are available and a phase-coherent central filtering is used. To filter the position at index p, $m+1$ position vectors $[{}^F_G\mathbf{P}_{p-m/2} \cdots {}^F_G\mathbf{P}_p \cdots {}^F_G\mathbf{P}_{p+m/2}]$ from the Seam Trajectory Buffer are used to find the polynomial coefficients $\mathbf{a}_0$ to $\mathbf{a}_n$. These coefficients are computed in such a way that the error criterion

$$\sum_{j=p-m/2}^{p+m/2} |\mathbf{P}(j) - {}^F_G\mathbf{P}_j| \tag{18}$$

is minimised in a least squares sense.

To filter the orientations of the seam locations a simple but effective approach is used. At index p, the orientations from index

$p-m/2$ to index $p+m/2$ are available, therefore the elements of the quaternion representations (Craig, 1986; Khalil & Dombre, 2002) of the $m+1$ orientations are simply averaged and normalised, which nicely smoothes the orientation. Suppose $\mathbf{Q}_p$ is the quaternion representation of rotation matrix ${}^{F}_{G}\mathbf{R}_p$ at index p, the quaternion average $\mathbf{Q}_p^{\text{avg}}$ equals

$$\mathbf{Q}_p^{\text{avg}} = \frac{\sum_{j=p-m/2}^{p+m/2} \mathbf{Q}_j}{m+1}, \tag{19}$$

and the normalised quaternion average $\mathbf{Q}_p^{\text{navg}}$ equals

$$\mathbf{Q}_p^{\text{navg}} = \frac{\mathbf{Q}_p^{\text{avg}}}{|\mathbf{Q}_p^{\text{avg}}|}. \tag{20}$$

Formulae to convert rotation matrices to quaternions and vice versa can be found in common textbooks on robotics (Craig, 1986; Khalil & Dombre, 2002).

4.6. Stability

With the filter procedure of the previous section a smooth robot motion is expected during which the seam-tracking sensor measures the remaining required path corrections. To achieve this smooth motion, the overall system with the trajectory-based control must be (closed-loop) stable as well. In the block diagram of Fig. 2 two loops can be distinguished: the inner loop of the Joint Motion Controller and at a higher level the outer loop of the trajectory-based control scheme.

The stability of the inner loop with the Joint Motion Controller during normal operation of the robot is assured by the manufacturer. A typical closed-loop bandwidth for this loop is about 10 Hz. In combination with the outer loop its stability is hardly affected as the trajectory-based control operates at significantly lower frequencies. Consider e.g. a sensor look-ahead distance of about 50 mm and a velocity of 100 mm/s. In this case there is a time delay of about 0.5 s between the measurement of a seam location by sensor and the instant when it is used by the Setpoint Generator.

With a stable inner loop, the smoothness of the motion depends mainly on the filtering of the measured setpoints. This is particularly relevant during the second part of real-time seam-tracking where the laser tool frame has to track the adjusted seam trajectory and future seam locations must be in the field-of-view of the sensor. If too noisy sensor data are used to determine the adjusted seam locations, vibrations may be induced in the robot motion and next measurements may be even noisier, etc. As was outlined in the previous section, filtering is applied by fitting a polynomial through a fixed number of points of which it is guaranteed that they span a minimal length of the seam. Setting the number of data points for the fit is a trade-off between more noise reduction and the capability to process more irregular seams. In practice, precise settings depend therefore on the sensor measurement noise level and the seam geometry. Typical filter parameters are given in Section 5.

4.7. Limitations

The following limitations need to be kept in mind, when using the trajectory-based control approach for real-time seam tracking:

- The seam trajectory cannot be tracked if no solution exists for correcting the orientation of a seam location in such a way that the sensor is positioned on the nominal seam trajectory. This may happen if the curvature at some parts of the seam trajectory is smaller than the look-ahead-distance.
- If the current robot location is close to the last location in the Tool Trajectory Buffer, the Setpoint Generator will start the deceleration phase and will not allow to add locations to the Tool Trajectory Buffer anymore. The risk that this may happen is larger if the look-ahead-distance is small at high robot speeds or if the average time for calculating the orientation correction, filtering and safety checks takes more than the available cpu-time.

5. Experimental results

In this section, the results of several teaching and tracking experiments will be presented and compared. Two different seam trajectories will be used. These are shown in Fig. 6.

These seams have been manufactured by laser cutting of sheet metal. A goal of the experiments is to obtain the accuracy of the laser focal point with respect to the seam trajectory. To do this a dummy laser welding head has been manufactured (Fig. 7), where the sensor can be mounted on different positions with respect to the robot flange. One of these positions represents the sensor tool frame and another represents the position of the laser focal point during welding. The distance between these tool positions represents the sensor look-ahead distance and is about 54 mm.

For each trajectory, both a 'teaching' and a 'tracking' experiment are performed. During the 'teaching' experiments, the actual seam trajectory is found by moving the sensor along the nominal seam trajectory. During this movement, the measured seam locations are stored in the Seam Trajectory Buffer. After the movement has completed, the seam locations in the Seam

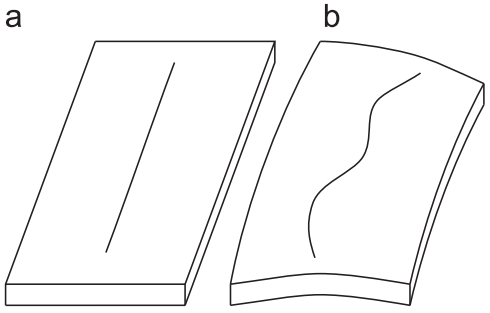

Fig. 6. Case seams: (a) line, (b) curved sine.

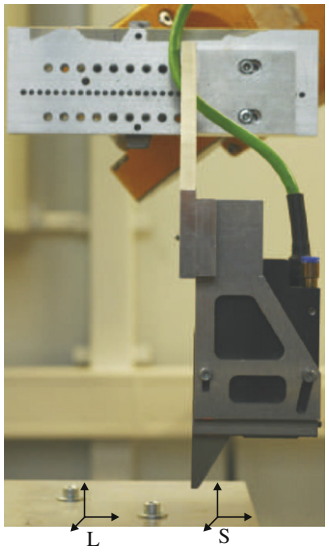

Fig. 7. Dummy head. The sensor can be mounted on different positions with respect to the robot flange.

Trajectory Buffer are filtered and added to the Tool Trajectory Buffer. The welding of the taught trajectory is subsequently measured in an additional processing step by mounting the sensor at the position of the laser tool frame and moving it along the locations in the Tool Trajectory Buffer.

In the 'tracking' experiments, the orientations of the measured seam locations are corrected and the result is filtered and added to the Tool Trajectory Buffer in one processing step. With the dummy head, the sensor can only be on one position at a time, so the tracking of the welding tool frame is measured by replaying the unaltered trajectory of the 'tracking' experiment after the sensor is positioned in the laser tool frame. The parameters for the 'teaching' and 'tracking' experiments are given in Table 1.

5.1. Line trajectory

The nominal trajectory for the line trajectory consists of two seam locations, one at the start and one at the end of the trajectory.

Teaching experiment: After the 'teaching' experiment has completed, the taught trajectory has been replayed with the sensor still mounted at the sensor tool frame position of the dummy welding head. Fig. 8(a) shows that the sensor measurements during replay with the sensor tool frame are within 0.05 mm, approaching the sum of the robot repeatability (0.025 mm) and the sensor resolution (0.025 mm in the y-direction). This shows that the teaching procedure is correct and that accurate welding results can be obtained with a welding head, which has the laser and sensor tool frame at the same position.

Next, the taught trajectory has been replayed with the sensor mounted at the laser tool position of the dummy welding head. Fig. 8(b) shows that the sensor measurements are mainly within 0.1 mm, which shows that the welding accuracy is well suited for laser welding. The slight increase in the measurements is attributed to small errors between the real robot system and the Direct and Indirect Geometric Model and/or the tool transformations. In the previous experiment such errors have no effect as these are cancelled as long as frames ${}^{F}_{T}\mathbf{T}_k$ and ${}^{F}_{S}\mathbf{T}_k$ in Fig. 2 are equal. If the seam locations are measured with a different tool transformation than the one that is used during replay, the robot joint angles are different for both motions. For this case, De Graaf (2007) showed with simulations that the geometric errors lead to tracking errors even for a perfect sensor system.

Tracking experiment: After the real-time 'tracking' procedure has completed, the tracked trajectory has also been replayed with the sensor mounted at the sensor position and the laser position of the dummy welding head. Fig. 9(a) shows the sensor measurements during replay with the sensor mounted in the original sensor tool frame are again mainly within 0.05 mm. Fig. 9(b) shows the sensor measurements during replay with the sensor mounted at the laser tool frame position of the dummy welding head. The measurements on the right are somewhat larger than the ones on the left, but still mainly within 0.1 mm. These results are very similar to the results that are achieved with the 'teaching' experiment as almost no orientation corrections are needed for a line trajectory.

Table 1
Parameters used during the teaching and tracking experiments.

Parameter	Line	Curved
Velocity (mm/s)	100	50
Minimal location distance for Seam Trajectory Buffer (mm)	0.2	0.2
Minimal location distance for Tool Trajectory Buffer (mm)	10	3
Fit order (Eq. (17))	2	2
Fit points m	32	32

5.2. Curved sine trajectory

To obtain a nominal trajectory for the curved sine trajectory, a point-to-point teaching procedure is used (De Graaf, Aarts, Meijer, & Jonker, 2004).

Teaching experiment: Fig. 10(a) shows the sensor measurements during replay with the sensor still mounted at the sensor tool frame position of the dummy welding head. These measurements are mainly within 0.2 mm, which is appropriate for laser welding at the sensor tool frame location. Fig. 10(b) shows the sensor measurements during replay with the sensor mounted at the laser tool frame location of the dummy welding head. The inaccuracy increases again in this case, some errors are about 0.3 mm, which is more than the tight requirement of 0.2 mm mentioned in the Introduction. As a result, some welds may fail, but this accuracy is still quite useful for laser welding of a wide range of industrial products, e.g. using larger focal distance.

Tracking experiment: The sensor measurements during replay of the tracked seam trajectory are shown in Fig. 11. The errors during replay with the sensor mounted in the original sensor tool frame in Fig. 11(a) are mainly within 0.4 mm. The errors during replay with the sensor mounted at the laser tool position of the dummy welding head in Fig. 11(b) are somewhat larger (mainly within 0.5 mm). In both cases, the accuracy is considerably worse than the requirement of 0.2 mm, which is attributed to geometric robot errors again. In this case of a curved seam trajectory, it is

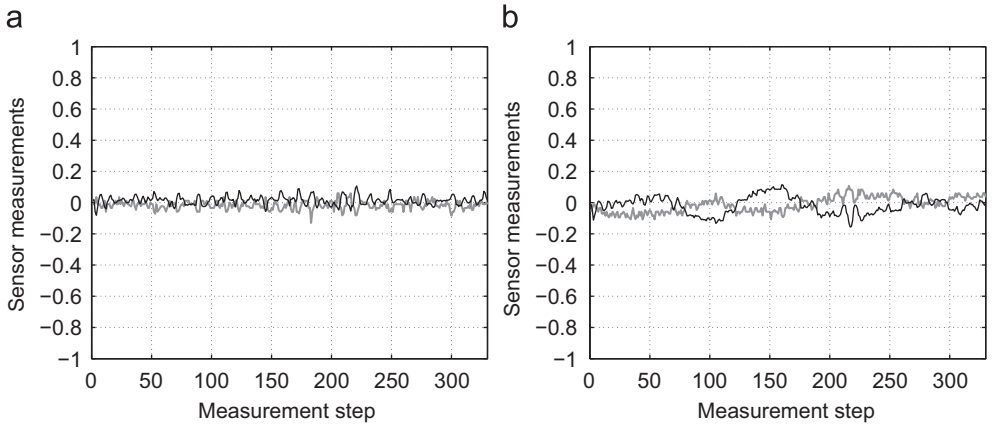

Fig. 8. Real-time teaching experiment of the line trajectory (—— s_z, —— s_y). (a) Replay with sensor tool frame, (b) replay with laser tool frame.

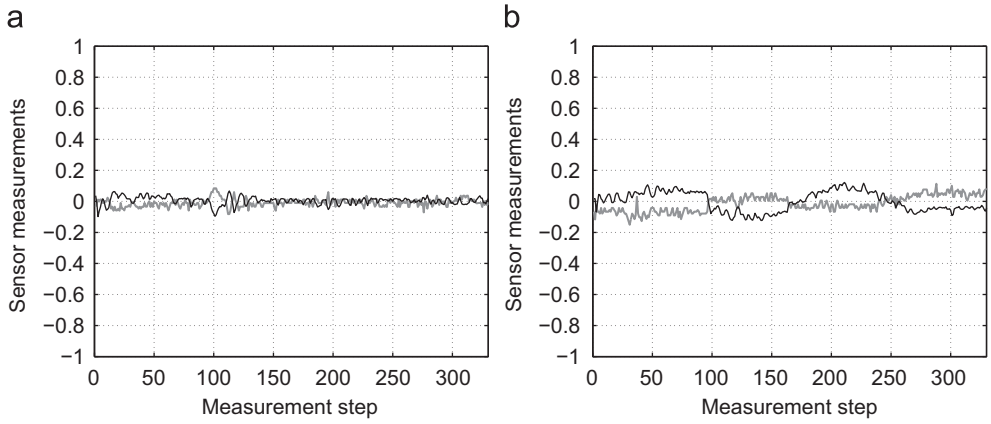

Fig. 9. Real-time tracking experiment of the line trajectory (—— s_z, —— s_y). (a) Replay with sensor tool frame, (b) replay with laser tool frame.

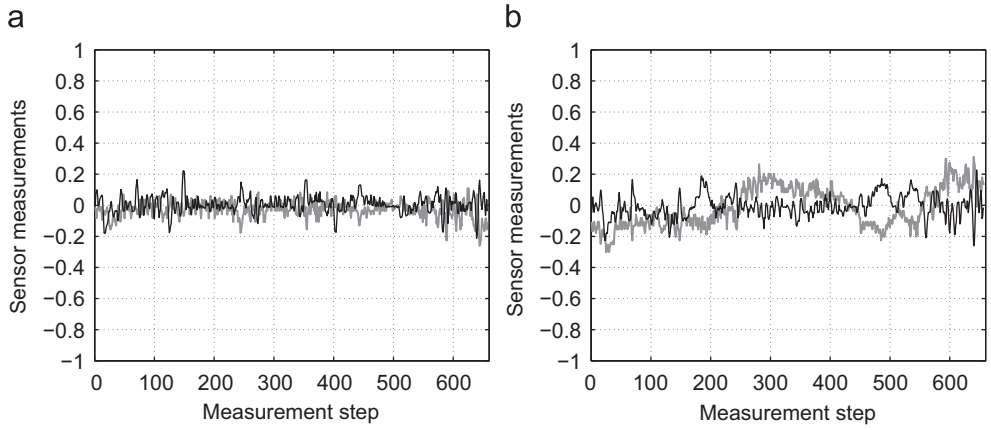

Fig. 10. Real-time teaching experiment of the curved sine trajectory (—— s_z, —— s_y). (a) Replay with sensor tool frame, (b) replay with laser tool frame.

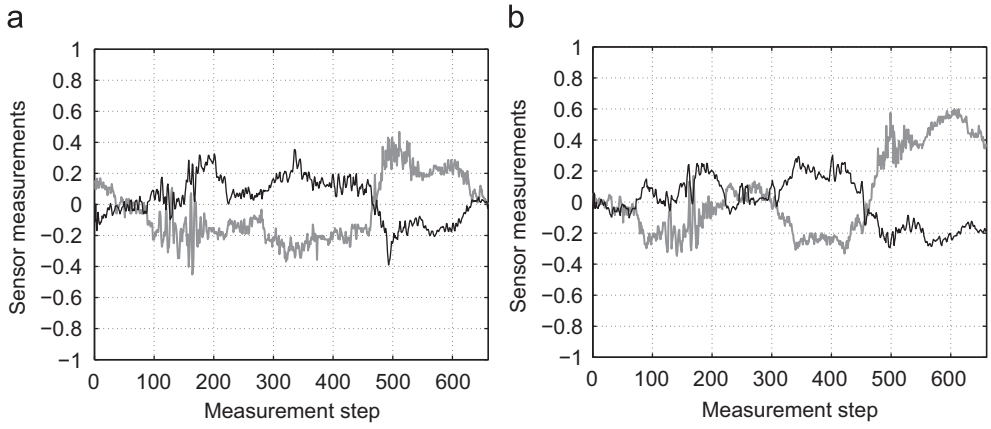

Fig. 11. Real-time tracking experiment of the curved sine trajectory (—— s_z, —— s_y). (a) Replay with sensor tool frame, (b) replay with laser tool frame.

caused by the robot orientation during the sensor measurements being different from the robot orientation when the laser tool frame reaches the measured location (De Graaf, 2007).

6. Discussion

A real-time seam tracking algorithm has been implemented using the trajectory-based control approach. This trajectory-based control architecture has several advantages over the time-based visual servoing methods that are frequently used in industry. To be able to use it a real-time Setpoint Generator and a method to synchronise the robot joint measurements and the sensor image acquisition are needed. The orientation of the synchronised locations is adapted to keep the sensor within the field-of-view of the nominal seam trajectory when the laser reaches the synchronised location. The control loop is closed by filtering the corrected locations and adding the filtered locations to the Tool

Trajectory Buffer. The experiments show that the trajectory-based control approach is well suited for real-time seam tracking.

Real-time teaching and real-time tracking experiments have been performed using a line trajectory and a curved sine trajectory. From these experiments the following conclusions can be drawn:

- The real-time seam tracking procedure is well suited for welding of moderately curved seam trajectories. The procedure is fast, because measuring and welding are done simultaneously in the same processing step. The procedure requires a sensor that measures ahead of the laser focal point. The obtained accuracy depends on the orientation correction, which is a function of the curvature of the seam trajectory. They range from 0.1 mm for a line trajectory to 0.5 mm for the curved sine trajectory.
- The real-time teaching procedure is well suited for accurate welding of heavily curved seam trajectories, provided that the measurements and corrections are done with the same tool frame transformations (small or zero look-ahead distance). The procedure requires two processing steps, first measuring, then welding. Accuracies better than 0.1 mm are achieved, which are almost independent of the curvature of the seam trajectory.

A further improvement of the accuracies can be achieved by using more precise geometric robot models.

References

Abo-Hammour, Z. S., Mirza, N. M., Mirza, S. M., & Arif, M. (2002). Cartesian path generation of robot manipulators using continuous genetic algorithms. *Robotics and Autonomous Systems*, *41*, 179–223.

Abramowitz, M., & Stegun, I. A. (1972). *Handbook of mathematical functions with formulas, graphs and mathematical tables*. New York: Dover Publications.

Ahmed Bazaz, S., & Tondu, B. (1999). Minimum time on-line joint trajectory generator based on low order spline methods for industrial manipulators. *Robotics and Autonomous Systems*, *29*, 257–268.

Andersen, H. J. (2001). *Sensor based robotic laser welding—Based on feed forward and gain scheduling algorithms*. Ph.D. thesis, Aalborg University.

Bae, K. Y., Lee, T. H., & Ahn, K. C. (2002). An optical sensing system for seam tracking and weld pool control in gas metal arc welding of steel pipe. *Journal of Materials Processing Technology*, *120*, 458–465.

Barnhill, R. E., & Riesenfled, R. F. (1974). *Computer aided geometric design*. New York: Academic Press.

Corke, P. I. (1994). *High-performance visual closed-loop robot control*. Ph.D. thesis, University of Melbourne, Department of Mechanical and Manufacturing Engineering.

Craig, J. J. (1986). *Introduction to robotics: Mechanics and control*. Boston: Addison-Wesley Publishing Company, Inc.

De Graaf, M. W. (2007). *Sensor-guided robotic laser welding*. Ph.D. thesis, University of Twente.

De Graaf, M. W., Aarts, R. G. K. M., Jonker, J. B., & Meijer, J. (2006). Real-time trajectory generation for sensor-guided robotic laser welding. In *Proceedings of the symposium on robot control* (*Syroco*) *2006*, Bologna: IFAC.

De Graaf, M. W., Aarts, R. G. K. M., Meijer, J., & Jonker, J. B. (2004). Modeling the seam teaching process for robotic laser welding. In P. Drews (Ed.), *Proceedings of the mechatronics and robotics 2004 conference*, September. APS-European Centre for Mechatronics.

De Graaf, M. W., Aarts, R. G. K. M., Meijer, J., & Jonker, J. B. (2005). Robot-sensor synchronization for real-time seam tracking in robotic laser welding. In *Proceedings of the third international WLT-conference on lasers in manufacturing*, Munich.

Fridenfalk, M., & Bolmsjö, G. (2003). Design and validation of a universal 6d seam tracking system in robotic welding based on laser scanning. *Industrial Robot: An International Journal*, *30*(5), 437–448.

Huissoon, J. P. (2002). Robotic laser welding: Seam sensor and laser focal frame registration. *Robotica*, *20*, 261–268.

Khalil, W., & Dombre, E. (2002). *Modeling, identification and control of robots*. London: Hermes Penton Ltd.

Kim, J. S., Son, Y. T., Cho, H. S., & Koh, K. I. (1996). A robust visual seam tracking system for robotic arc welding. *Mechatronics*, *6*, 141–163.

Kim, P., Rhee, S., & Lee, C. H. (1999). Automatic seam teaching of welding robot for free-formed seam using laser vision system. *Optics and lasers in engineering*, *31*, 173–182.

Liu, Y., Hoover, A. W., & Walker, I. D. (2004). A timing model for vision-based control of industrial robot manipulators. In *IEEE transactions on robotics*.

Nayak, N., & Ray, A. (1993). *Intelligent seam tracking for robotic welding. Advances in industrial control*. Berlin: Springer-Verlag.

Sanderson, A. C., & Weiss, L. E. (1980). Image-based visual servo control using relational graph error signals. In *Proceedings of the international conference on cybernetics and society*, Cambridge.

Sgarbi, F., & Cammoun, R. (1992). Real time trajectory generation using filtering techniques. In *Proceedings of the 2nd international conference on automation, robotics and computer vision*, Singapore.

Yu, J. Y., & Na, S. J. (1997). A study on vision sensors for seam tracking of height-varying weldment. Part 1: Mathematical model. *Mechatronics*, *7*, 599–612.

Yu, J. Y., & Na, S. J. (1998). A study on vision sensors for seam tracking of height-varying weldment. Part 2: Applications. *Mechatronics*, *8*, 21–36.